Journal of Photochemistry and Photobiology A: Chemistry 233 (2012) 53–59

Contents lists available at SciVerse ScienceDirect

Journal of Photochemistry and Photobiology A: Chemistry

journal homepage: www.elsevier.com/locate/jphotochem

2-Chlorophenol degradation via photo Fenton reaction employing zero valent iron nanoparticles

Guadalupe Beatriz Ortiz de la Plata*, Orlando Mario Alfano, Alberto Enrique Cassano

INTEC (Universidad Nacional del Litoral – CONICET), Colectora de Ruta Nacional N° 168, Km. 472, 5, 3000 Santa Fe, Argentina

ARTICLE INFO

Article history:
Received 2 September 2011
Received in revised form 7 February 2012
Accepted 18 February 2012
Available online 27 February 2012

Keywords:
Heterogeneous photo Fenton
Zero valent iron
2-Chlorophenol
Optical properties
Radiation field

ABSTRACT

In the present work the influence of various factors on the degradation of 2-chlorophenol (2-CP) via heterogeneous photo Fenton reaction using zero valent iron (ZVI) nanoparticles as a source of iron was studied. The results were compared with those obtained using goethite as a reservoir of iron.

During the study the pH, catalyst loading and the level of irradiation were varied. In the results it can be observed: (i) a high dependence of the working pH, rendering better results as pH decreases, (ii) a great improvement in conversion by applying radiation, as compared with the data obtained under dark conditions, (iii) an interesting non-linearity between conversion and catalyst loading, which can be partially explained by estimating the average radiation absorption available in the reactor for different catalyst loads, using the information given by the optical properties of ZVI.

1. Introduction

Resulting from the increasing influence of human activities, persistent contamination in ground and municipal waste waters has become a problem of high priority, that needs the development of decontaminating technologies appropriate for those refractory contaminants.

The so called Advanced Oxidation Processes (AOPs), are particularly attractive as methods of destruction of recalcitrant pollutants in waters. Among them can be mentioned the Fenton reactions that employ hydrogen peroxide and iron compounds in order to produce the unselective and highly oxidant hydroxyl radicals. A remarkable difference between Fenton processes and other AOPs technologies, is that in this kind of processes hydroxyl radical generation can be improved by two different ways: (1) the irradiation of the media by UV/Vis radiation (photo-Fenton processes) [1,2] and (2) the improvement coming from increasing temperature [3,4]. These two enhancements can be achieved simultaneously employing solar irradiation [5]. The heterogeneous Fenton processes employ hydrogen peroxide and a solid iron container/carrier, for the hydroxyl radical production, in order to avoid complex post treatment processes [6–9]. Most Heterogeneous photo-Fenton catalysts also present the advantages of solar applicability and temperature improvement.

In the last decade a large group of heterogeneous catalysts has been studied for application in Fenton and Photo Fenton Processes [8] in order to incorporate iron to the system, resorting to either different supports to immobilize the solid or compact iron aggregations such as different forms of iron oxides. Among the compounds that have been examined can be mentioned: membranes [10], alginates [11], silica [12,13], zeolites [14,15], alumna [16], glass [17], activated carbon [18], and clays like bentonites and laponites [6,19,20] or natural clays [21]. The second option includes synthesized as well as natively found iron oxides [13,16,22–26]. Among the last ones is remarkable the use of goethite [7,8,20,27–30]. Also bimetallic (mostly Cu/Fe) heterogeneous Fenton catalysts have been studied [31].

Most recently have appeared various studies that employ zero valent iron (ZVI) coming from different sources and various granulometries. These materials can be used in advanced oxidation Fenton technologies, or as reductive agents, combined or not with UV radiation [32–34]. They can be used in different forms: such as bars [35], particles [34,36–38], wool [39] and, most recently, nanoparticles [33,36,38,40].

Employing ZVI presents, as advantages respect to the iron oxide solids utilization, much higher reaction rates of contaminant decomposition, under certain operating conditions, the possibility of degradation of contaminants by the reductive properties of ZVI and its relatively low cost.

Although in the literature there are several works employing radiation combined with ZVI [33,37,40–43], the employed radiation includes low wavelengths that can produce simultaneously hydrogen peroxide photolysis and do not allow to discriminate both

* Corresponding author. Tel.: +54 0 342 451 1546; fax: +54 0 342 451 1087.
E-mail address: guadaortiz@santafe-conicet.gov.ar (G.B. Ortiz de la Plata).

1010-6030/$ – see front matter © 2012 Elsevier B.V. All rights reserved.
doi:10.1016/j.jphotochem.2012.02.023

phenomena. Also, the knowledge of the local rate of photon absorption is essential for obtaining kinetic expressions independent of the experimental device, and for designing purposes [44].

2-Chlorophenol (2-CP) is used as germicide/disinfectant and as a precursor for synthesizing pesticides and other chlorophenols. It can also be produced as a byproduct in water disinfection and in pulp bleaching [45].

The present work studied the influence of several operating variables in the degradation of 2-CP by the heterogeneous photo Fenton reaction employing ZVI nanoparticles as source of iron. Also, the results were compared with those obtained employing goethite.

2. Materials and methods

2-CP 99%+, chlorobenzoquinone (ClBQ) 95%+ and chlorohydroquinone (ClHQ) 85%+ were provided by Aldrich. H_2O_2 was supplied by Cicarelli (ACS, 30%). The pH was adjusted with perchloric acid (ByA, ACS, 70%). The ZVI nanoparticles employed in this work were produced by Nanotek S.A. (www.nanoteksa.com), according to a proprietary novel technology based on chemical reduction of ferric salts with borohydride in a stabilized multiphase nanoemulsion [33]. The product is obtained as an aqueous black suspension, and the particles have magnetic properties.

The work was performed in a cylindrical, well-stirred, batch reactor irradiated from a transparent radiation bottom, which was illuminated with a tubular lamp placed at the focal axis of a parabolic reflector [7]. The reactor was also equipped with internal glass heat exchangers connected to a thermostatic bath for controlling temperature and an external insulation made of K-Wool. The described device allows to irradiating the suspension with photons whose wavelength ranges goes from 340 to 410 nm, range that can be expanded to higher wavelengths by changing the lamp, for example for one that simulates the solar spectrum.

The reactor was filled with distilled water. Then, 2-CP was added to reach an initial concentration of 0.39 mM (50 ppm). After attaining steady-state temperature (and when corresponds, lamp stabilization), the prescribed H_2O_2 and the desired concentration of ZVI was incorporated to the system. The pH was adjusted to 3 with perchloric acid, except for the run performed at the natural pH of the suspension (6.3). The range of the initial molar ratio of $C_{H_2O_2,0}$ to $C_{2\text{-CP},0}$ (R), was set in approximately 13 (the stoichiometric ratio); the catalyst loading was varied in four levels from 0 to 44 ppm of iron, measured by AA after digestion of the sample [46] and the temperature was set at 25 °C. Irradiation was varied in two levels, 0 and 100% referred to the maximum input power, measured by actinometry.

Each experimental run lasted for 3 h. During this period samples were extracted at prefixed times. Analysis in each sample was carried out for: Total Organic Carbon (TOC), 2-CP concentration, total dissolved iron (Fe_D) and hydrogen peroxide concentration.

2-CP concentration was monitored with HPLC (Waters) equipped with a LC-18 Supelcosil reversed-phase column. The eluent was a ternary mixture of water (containing 1% v/v acetic acid), methanol, and acetonitrile (60:30:10), pumped at a rate of 1 mL min^{-1}, retention times for ClBQ, ClHQ and 2-CP, 6, 7.5 and 11 min respectively. TOC was measured with a Shimadzu TOC-5000 Analyzer. H_2O_2 was measured spectrophotometrically with a modified iodometric technique [47] with a Cary 100 Bio spectrophotometer. Total iron content in the solution was measured by AA (Perkin Elmer A Analyst 800). Before analysis, solid particles were separated by filtration with Whatman Syringe filters of 0.02 μm, after quenching HPLC samples with an equivalent volume of methanol.

The question of the chemical and mechanical stability of zero-valent iron nanoparticles is an important issue. Several authors have indicated that zero-valent nano sized iron particles are not stable in water and are oxidized to iron oxides [35,48,49]. The composition of these iron oxides depends on many factors; among them the pH and the preparation method employed to produce the said particles. In any event, they form a sort of protective film that avoids further oxidation. At alkaline pH this compound seem to be ferrous iron hydroxide. It has been proposed that under acidic conditions, this layer is a source of Fe^{3+} ions to the solution that, upon reduction, tend to accelerate the Fenton mechanisms. On the other hand, the pH has a very strong influence on the particles mechanical stability. The isoelectric point of iron nanoparticles has been determined as equal to 8.3 [50]. The influence of the pH on the ζ potential of iron nano particles is very significant [48] either above or below the isoelectric point. However in spite that at pH = 3 (our work) the ζ potential is very large, some sort of agglomeration was still observed in this work. This could be due to the increase in the medium pH produced by the addition of iron nanoparticles [48], but this effect cannot be too significant at the very low iron concentration that has been employed here (not larger than 44 ppm).

Table 1
Typical run conditions and results for 3 H of reaction time.

Fe_{Tot} [a] (ppm)	pH	% Rad.	*R*	X_{2CP} (%)	X_{TOC} (%)	$X_{H_2O_2}$ (%)
45	3	100	13	75	15	12
44	3	0	13	0 [b]	0 [b]	7.8
44	6.3	100	13.1	0 [b]	0 [b]	16.8
18	3	100	13.7	82.7	4.5	18.4
6	3	100	13.5	33.5	0.2	2.91[e]
0.3×10^2 [c]	3	100	50	41.5 [d]	21.8 [d]	43.1 [d,e]

[a] Fe_{Tot} Total iron content in the suspension. Since in all the runs the dissolved iron measurements (Fe_D) were below the detection limit, the Fe_{Tot} corresponds almost completely to the catalyst loading employed in the experience.
[b] For the zero conversion values, in all runs, the obtained RSD% has been lower than 3% for all HPLC and TOC measurements.
[c] Goethite load g/L. Iron equivalent for 0.5 g/L load ppm.
[d] For 6 h of reaction time.
[e] Detected ClHQ by HPLC.

3. Results and discussion

Table 1 shows the list of experimental conditions employed and percentage conversions obtained after 3 h of reaction time. In all cases total dissolved iron measurements resulted lower than the AA detection limit (<0.1 ppm). In the runs with higher catalyst load, traces of chlorobenzoquinone (ClBQ) were observed by HPLC.

Fig. 1 shows the experimental results as dimensionless concentrations vs. time for a typical run. As expected, an increase on the rate of degradation of 2-CP with reaction time can be observed.It may be noted that although the concentration of 2-CP significantly decreases, it does not occur the same with TOC, which indicates the

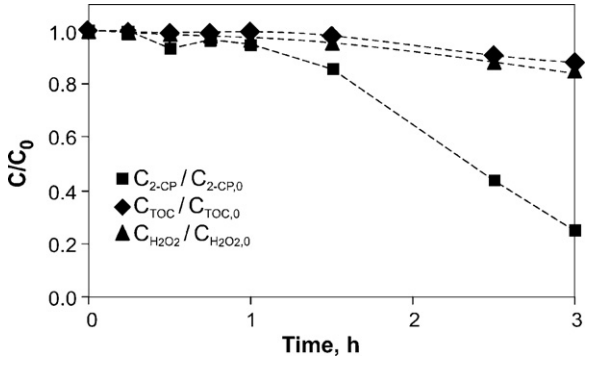

Fig. 1. Dimensionless concentrations vs. time. ~44 ppm Fe_{Tot}, pH = 3, $R \sim 13$ and 100% irradiation.

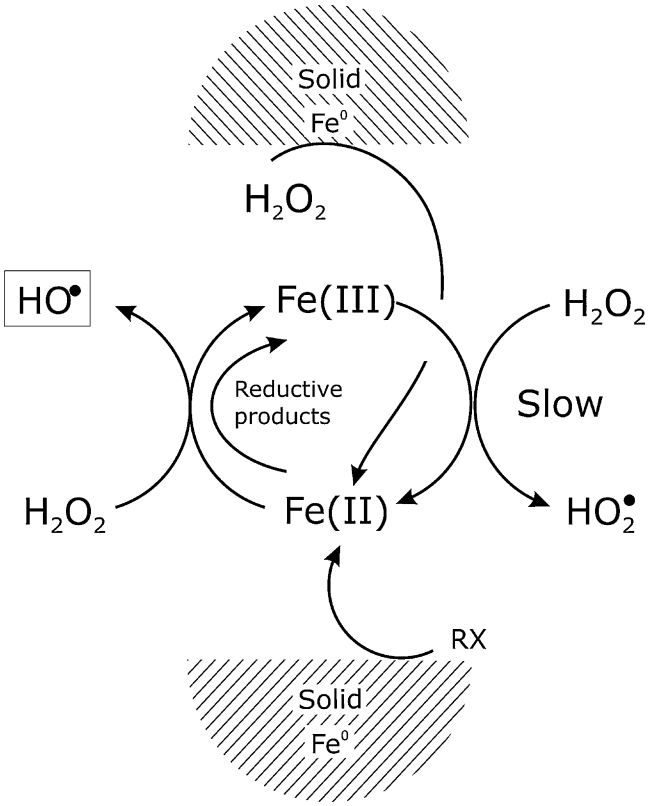

Fig. 2. Mechanism description.

existence of intermediate products of reaction that have not been degraded.

The observed behavior can probably be explained by the reaction mechanism proposed by Bergendahl and Thies [51]. In this work, an initial step of ZVI dissolution is proposed as an oxidation reaction. This reaction would partially explain the lag period observed in Fig. 1:

$$Fe^0 + H_2O_2 \rightarrow Fe^{2+} + 2HO^- \quad (1)$$

Reaction (1) would be followed by the classic steps corresponding to the Homogeneous Fenton reactions, among which stand out:

$$Fe^{2+} + H_2O_2 \rightarrow Fe^{3+} + HO^- + HO^\bullet \quad (2)$$

$$Fe^{3+} + H_2O_2 \rightarrow Fe^{2+} + H^+ + HO_2^\bullet \quad (3)$$

A more complete mechanism of the homogeneous degradation of 2-CP through heterogeneous photo-Fenton reactions can be seen in previous works of the authors [7,8]. The basic idea of the mechanism is shown in Fig. 2.

Considering the runs carried out in the dark (0% irradiation) maintaining the same conditions for the remaining parameters (Table 1), only small concentration of hydrogen peroxide consumption can be observed, leaving 2-CP concentration almost unchanged during the run, with no observed tendencies.

This important difference is produced because, under irradiation, steps related to the interaction of the dissolved iron and radiation occur, accelerating the production of the hydroxyl radicals and leading to major conversions of 2-CP.

$$Fe(OH)^{+2} \xrightarrow{h\nu} Fe^{2+} + HO^\bullet \quad (4)$$

It should be remarked that, for the interpretation of this part of the mechanism, the knowledge of the radiation field inside the reactor is necessary, considering simultaneously the homogeneous species and the heterogeneous suspension [7].

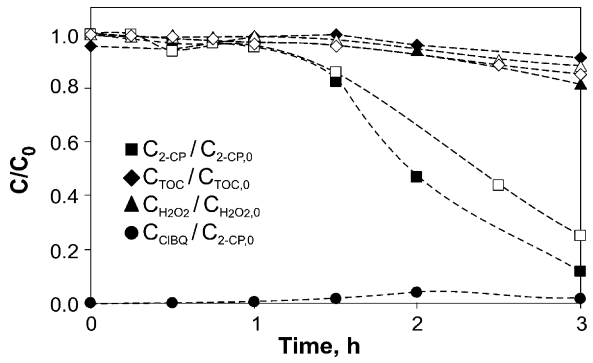

Fig. 3. Dimensionless concentrations vs. time. Filled symbols: 18 ppm Fe_{Tot}. Open symbols: comparison with results shown for 44 ppm Fe_{Tot}.

3.1. Effect of pH

Working at the natural pH of the suspension (pH = 6.3) no conversion of 2-CP was observed. The RSD% was lower than the error of the employed analytic technique not showing a definite tendency.

This effect can be explained because in the other runs most of the contaminant destruction occurs due to the homogeneous part of the mechanism; these reactions are highly sensitive to the working pH, having an optimal result at pH = 2.8 [9].

3.2. Effect of the catalyst loading

In Figs. 3 and 4 the effect of the variation in the catalyst load on the reaction behavior can be observed.

The appearance of ClBQ in Fig. 3 can be explained by the reactions produced by 2-CP degradation in the homogeneous phase. These reactions play a very significant role in the enhancement of the transformation of Fe^{3+} to Fe^{2+} according to the scheme shown below, proposed and validated for phenol by Chen and Pignatello [52,53] and modified for 2-CP by Ortiz de la Plata [8]:

$$\begin{aligned} &HO^\bullet + 2-CP \rightarrow ClDHCD^\bullet \\ &Fe^{3+} + ClDHCD^\bullet \rightarrow Fe^{2+} + ClHQ \\ &Fe^{3+} + ClHQ \rightarrow Fe^{2+} + ClSQ^\bullet \\ &Fe^{3+} + ClSQ^\bullet \rightarrow Fe^{2+} + ClBQ \end{aligned} \quad (5)$$

where $ClDHCD^\bullet$, chlorodihydroxycyclohexadienyl radical; and $ClSQ^\bullet$, chlorosemiquinone radical.

The ClHQ has not been detected in all the experimental runs. This is more evident in the dark ones. In a previous work [8] those intermediates that could not be observed with HPLC were detected by Mass spectrometry. Observing the results, the larger

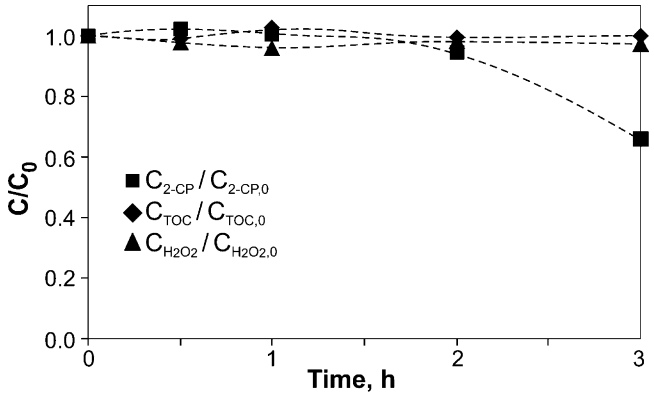

Fig. 4. Dimensionless concentrations vs. time. ppm Fe_{Tot} = 6, pH = 3, R = ~13 and 100% irradiation.

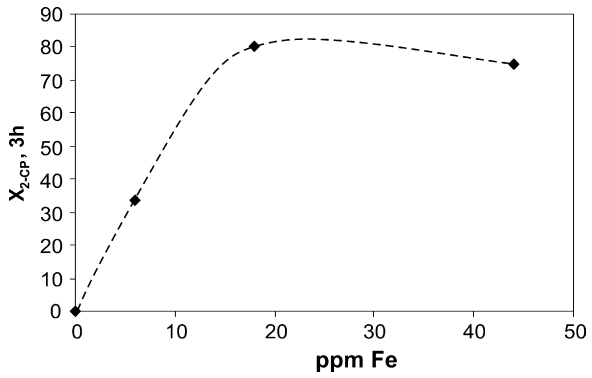

Fig. 5. Percentage conversion of 2-CP as function of catalyst load.

concentrations of ClHQ were observed at lower catalyst loading. This is very understandable; at larger reaction rates, the ClHQ will be decomposed more rapidly by the Fenton process. The presence of higher concentration of ClHQ in irradiated experiments is due to the existence of reactions that transform the ClBQ in ClHQ as a consequence of radiation absorption [52]:

$$\begin{aligned} &\mathrm{ClBQ} \xrightarrow{h\nu} \mathrm{ClSQ}\cdot + \mathrm{HO}\cdot \\ &\mathrm{Fe}^{2+} + \mathrm{ClSQ}\cdot \rightarrow \mathrm{Fe}^{3+} + \mathrm{ClHQ} \end{aligned} \tag{6}$$

Fig. 5 shows the percentage conversion of 2-CP as a function of the catalyst load. As can be seen in this figure, there exists an interesting non linearity between the obtained conversion and the employed catalyst load.

This can be partially explained by observing the available radiation in the reactor for different operating conditions, using the optical properties of ZVI. This parameter is defined as the local volumetric rate of photon absorption (LVRPA). In Table 1 and Fig. 5, it can be seen that the 2-CP conversion increases from Fe_{Tot} = 6 to 18 ppm and then, for Fe_{Tot} = 44 ppm the degradation is slightly lower. Considering that all the experimental runs were duplicated, possibly, although in a manner not totally conclusive, it can be affirmed that the curve insinuates the presence of a maximum. However, X_{TOC} (%) always increases, indicating that, to some extent, the oxidation stages of the degradation products are not much affected by this phenomenon. Probably, for higher catalyst loading, also a similar trend in the X_{TOC} (%) could have been observed.

3.3. Radiation field effects

For rather dilute suspensions (concentration of solids smaller than 5–10%) a pseudo-homogeneous system of the radiant field along a single direction of propagation in the three-dimensional space, can be described by the radiative transfer equation (RTE) [54,55]:

$$\begin{aligned} &\frac{dL_{\lambda,\underline{\Omega}}}{ds}(s,t) + \underbrace{\alpha_\lambda(s,t)L_{\lambda,\underline{\Omega}}(s,t)}_{\text{absorption}} + \underbrace{\sigma_\lambda(s,t)L_{\lambda,\underline{\Omega}}(s,t)}_{\text{out-scattering}} \\ &== \underbrace{\frac{\sigma_\lambda(s,t)}{4\pi}\int_{\Omega'=4\pi} B(\underline{\Omega}'\rightarrow\underline{\Omega})L_{\lambda,\underline{\Omega}}(s,t)\,d\underline{\Omega}'}_{\text{in-scattering}} \end{aligned} \tag{7}$$

where $dL_{\lambda,\underline{\Omega}}(s,t)/ds$ is the rate of change of the spectral specific intensity measured along the directional coordinate s, having a wavelength λ (between λ and $\lambda + d\lambda$) and a direction of radiation propagation characterized by the unit vector $\underline{\Omega}$. Emission has been neglected because photocatalytic reactions are performed at ambient temperature and all other forms of induced emission are non-existent. α_λ and σ_λ are the absorption and scattering linear volumetric coefficients and B is the phase function for elastic scattering that acts as a source of photons coming from any direction $\underline{\Omega}'$ to the direction under consideration $\underline{\Omega}$.

Once the spectral and directional distribution of radiation intensities is known, by solving Eq. (7), the spectral incident radiation that results from the integration of the specific intensities from all the contributing directions of radiation propagation ($\underline{\Omega}$) to the point under consideration located at position $\underline{x}$, can be readily calculated according to:

$$E_{p,\lambda,o}(\underline{x},t) = \int_{\Omega=4\pi} L_{\lambda,\underline{\Omega}}(\underline{x},t)\,d\underline{\Omega} \tag{8}$$

From Eq. (8), the important property responsible for activating the catalyst, the spectral Local Volumetric Rate of Photon Absorption (LVRPA) is obtained as follows:

$$L^a_{p,\lambda}(\underline{x},t) = \alpha_{\lambda,React}(\underline{x},t)E_{p,\lambda,o}(\underline{x},t) \tag{9}$$

In addition, for polychromatic radiation:

$$L^a_p(\underline{x},t) = \int_\lambda \alpha_{\lambda,React}(\underline{x},t)E_{p,\lambda,o}(\underline{x},t)d\lambda \tag{10}$$

where the subscript React. includes two possibilities: (i) a chemically active species capable of absorbing radiation and initiating a reaction and (ii) a catalyst with the quality of being able to become activated by the appropriate radiation absorbing process. The value of $L^a_p(x,t)$ represents the absorbed photons that initiate the reaction.

It is clear that to solve the RTE inside the reactor to calculate the LVRPA, the absorption coefficient α, the scattering coefficient σ and the phase function $B(\underline{\Omega}'\rightarrow\underline{\Omega})$ must be known for each relevant wavelength involved in the reaction.

The optical properties of ZVI were obtained during the course of this work, adapting the corresponding techniques previously reported [56]. The employed methodology is described in Fig. 6.

For the numerical resolution of the RTE the discrete ordinate method (DOM) was employed [57]. For the optimization procedure a non-linear multiparameter estimator based on the algorithm of Levenberg–Marquardt [58,59] was employed.

Following the work of Satuf et al. [60], the chosen phase function was the one parameter equation suggested by Henyey and Greenstein, the HG phase function [61]:

$$B_{HG,\lambda}(\mu_0) = \frac{(1-g_\lambda^2)}{(1+g_\lambda^2-2g_\lambda\mu_0)^{3/2}} \tag{11}$$

where g_λ is called the dimensionless asymmetry factor, and can be determined for each particular wavelength. According to the behavior of the suspension, the shape of the phase function can change.

In these experiments, Eq. (7) is simplified by the azimuthal symmetry of the radiation arriving to the reactor [62]. On that account, the analysis of the reactor can be reduced to a one-dimensional model in space and a one-directional model for radiation propagation.

With the above assumptions and considering the new form of the phase function, the RTE for the reactor becomes:

$$\mu\frac{dL_{\lambda,\underline{\Omega}}(x,\mu)}{dx} + \beta_\lambda I_{\lambda,\underline{\Omega}}(x,\mu) = \frac{\sigma_\lambda}{2}\int_{\mu'=-1}^{1} L_{\lambda,\underline{\Omega}}(x,\mu)B_\lambda(\mu,\mu')\,d\mu' \tag{12}$$

where $\mu = \cos\theta$ and θ is the angle of radiation propagation after scattering, measured from the Cartesian coordinate $\underline{x}$. $\beta_\lambda = \alpha_\lambda + \sigma_\lambda$ is the extinction coefficient.

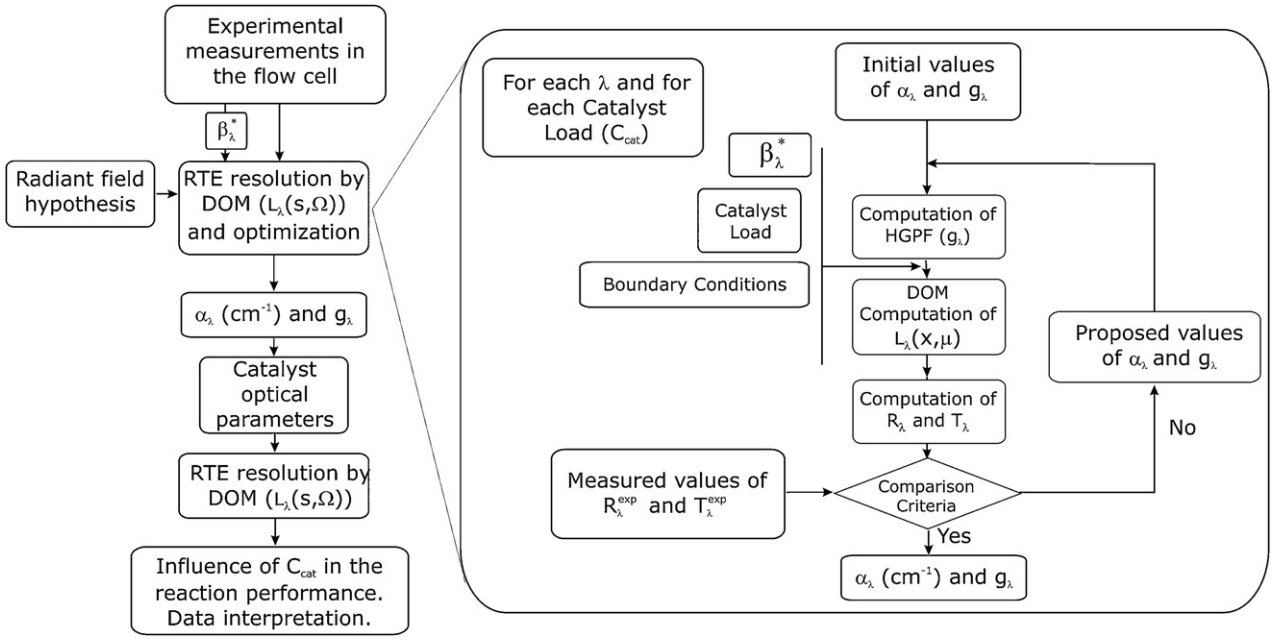

Fig. 6. Schematic description of the methodology for calculating optical properties.

Table 2
Optical properties of ZVI suspensions at pH 3.

λ, nm	α^*, $cm^2\ g^{-1}$	g	β^*, $cm^2\ g^{-1}$	σ^*, $cm^2\ g^{-1}$	$\omega = \sigma/\beta$
340	21,568	0.9611	24,095	2528	0.1049
345	21,346	0.9557	24,126	2779	0.1152
350	21,125	0.9504	24,156	3031	0.1255
355	20,904	0.9450	24,186	3282	0.1357
360	20,682	0.9396	24,216	3534	0.1459
365	20,815	0.9425	24,134	3319	0.1375
370	20,949	0.9454	24,052	3104	0.1290
375	21,082	0.9483	23,971	2888	0.1205
380	21,215	0.9513	23,889	2673	0.1119
385	20,088	0.9480	23,930	3842	0.1606
390	18,960	0.9447	23,971	5011	0.2090
395	17,832	0.9414	24,012	6180	0.2573
400	16,705	0.9381	24,053	7348	0.3055
405	16,397	0.9272	23,664	7267	0.3071
410	16,089	0.9162	23,275	7185	0.3087
415	15,782	0.9053	22,885	7104	0.3104
420	15,474	0.8944	22,496	7022	0.3121

The obtained optical properties are shown in Table 2 and Fig. 7.If the radiant field obtained by solving the RTE in the reactor is averaged over the reactor volume (L_R for the one dimensional model) and the polychromatic radiation emission is considered by integrating along the significant wavelengths, the averaged rate of polychromatic photon absorption inside the reactor is obtained by means of the following expression.

$$\left\langle L_p^a \right\rangle = \frac{1}{L_R}\int_0^{L_R}\int_\lambda \alpha_\lambda \int_{\Omega=4\pi} L_{\lambda,\underline{\Omega}}(x,\mu)\,d\Omega\,d\lambda\,dx \qquad (13)$$

Fig. 8 shows the obtained $\left\langle L_p^a \right\rangle$ as function of catalyst load. This figure presents a plateau in the value of the averaged LVRPA indicating that after a given catalyst loading (in the order of 30 ppm) the reactor shows some form of saturation that could even lead to a decrease in its degradation performance.There is another phenomenon that may produce the above mentioned decline in reactivity when the catalyst loading is increased. At high catalyst concentrations, mass transfer limitations can occur [63,64]. This phenomenon could explain the observed differences in the conversion curve in addition to the previously mentioned lack of radiation at high catalyst loads that renders dark regions in the reactor space.

3.4. Comparison with the same reaction employing goethite

Fig. 9 shows the comparison of the obtained results employing goethite and ZVI.

As shown in Table 1, it should be noticed that the required amount of hydrogen peroxide and the employed iron equivalent

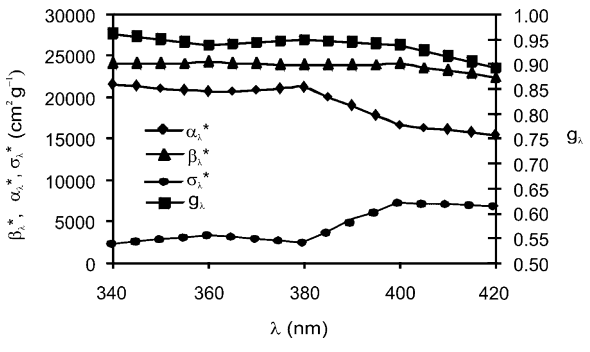

Fig. 7. Optical properties of ZVI suspension as function of wavelength.

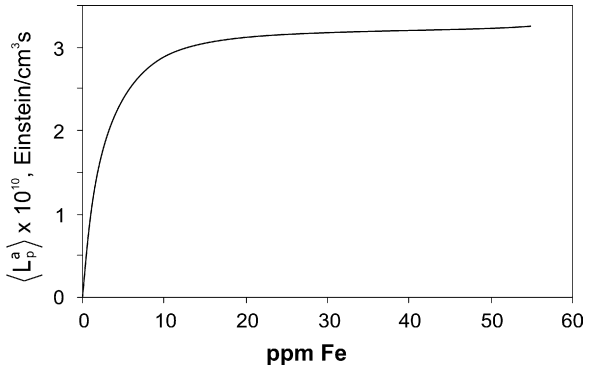

Fig. 8. Averaged LVRPA (Einstein/cm^3 s), as function of the catalyst load.

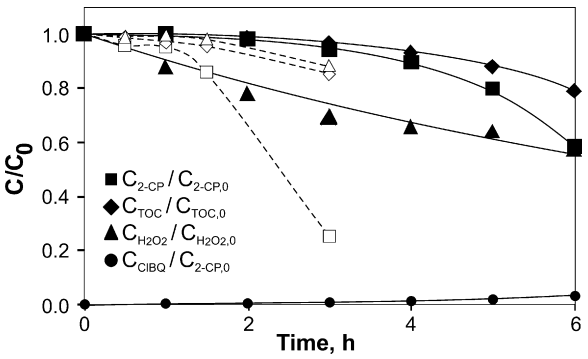

Fig. 9. Dimensionless concentrations vs. time. Open symbols: ~44 ppm Fe_{Tot}. $R \sim 13$ and Filled symbols: Goethite, 0.5 g/L, $R \sim 50$.

in the case of using goethite, are significantly different. It can be seen that, using ZVI larger conversions are obtained with a lower requirement of hydrogen peroxide. Approximately one fourth of the oxidant concentration is necessary for obtaining similar conversions in half of the time. This is a remarkable result in terms of process economics. It is necessary to emphasize that, in the case of employing ZVI nanoparticles, the remaining solution does not present traces of leached iron over the detection limits, 0.1 ppm.

4. Conclusions

From the reported results it can be concluded that:

(i) There is a high dependence of the reaction rate with the working pH, improving the reaction efficiency when the pH is decreased.
(ii) Comparing the results obtained when the reaction is carried out under dark conditions, there is a great improvement in the reaction conversion by applying radiation.
(iii) Comparing the efficiency of using ZVI with that obtained employing goethite, it can be concluded that: Similar conversions are achieved in half of the time necessary for the latter and there is a significantly less hydrogen peroxide concentration requirement; in fact, to reach similar conversions, it is sufficient to apply four times lower concentrations in the case of ZVI. Both variables are susceptible of further optimization.
(iv) The applied methodology has the important advantage of minimizing the iron leaching into the solution to concentrations lower than 0.1 ppm.
(v) An unusual non-linearity between the obtained conversion and the employed catalyst load was observed. This can be partially explained by estimating the average radiation absorption rate in the reactor for the different catalyst loads, employing the optical properties of the ZVI suspensions. Additionally, the possibility of mass transfer limitations at high catalyst loads will share the cause for the observed effect.

Acknowledgments

The authors thank Universidad Nacional del Litoral, Consejo Nacional de Investigaciones Científicas y Técnicas and Agencia Nacional de Promoción Científica y Tecnológica for their financial support. The authors gratefully thank Eng. Susana Gervasio for the AA analysis of the iron samples. The technical assistance Mr. Antonio Negro is also acknowledged.

References

[1] O. Gonzalez, C. Sans, S. Esplugas, S. Malato, Application of solar advanced oxidation processes to the degradation of the antibiotic sulfamethoxazole, Photochemical and Photobiological Sciences 8 (2009) 1032–1039.
[2] M. Zahorodna, E. Oliveros, M. Wörner, R. Bogoczek, A.M. Braun, Dissolution and mineralization of ion exchange resins: differentiation between heterogeneous and homogeneous (photo-)Fenton processes, Photochemical and Photobiological Sciences 7 (2008) 1480–1492.
[3] J. Farias, E.D. Albizzati, O.M. Alfano, Kinetic study of the photo-Fenton degradation of formic acid. Combined effects of temperature and iron concentration, Catalysis Today 144 (2009) 117–123.
[4] W. Gernjak, M. Fuerhacker, P. Fernandez-Ibañez, J. Blanco, S. Malato, Solar photo-Fenton treatment – process parameters and process control, Applied Catalysis B: Environmental 64 (2006) 121–130.
[5] J. Farias, E.D. Albizzati, O.M. Alfano, Modelling and experimental verification of a solar reactor for photo-Fenton treatment, Water Science and Technology 61 (2010) 1419–1426.
[6] J. Feng, X. Hu, P.L. Yue, S. Qiao, Photo Fenton degradation of high concentration Orange II (2 mM) using catalysts containing Fe: a comparative study, Separation and Purification Technology 67 (2009) 213–217.
[7] G.B. Ortiz de la Plata, O.M. Alfano, A.E. Cassano, Decomposition of 2-chlorophenol employing goethite as Fenton catalyst II: reaction kinetics of the heterogeneous Fenton and photo-Fenton mechanisms, Applied Catalysis B: Environmental 95 (2010) 14–25.
[8] G.B. Ortiz de la Plata, O.M. Alfano, A.E. Cassano, Decomposition of 2-chlorophenol employing goethite as Fenton catalyst. I. Proposal of a feasible, combined reaction scheme of heterogeneous and homogeneous reactions, Applied Catalysis B: Environmental 95 (2010) 1–13.
[9] J.J. Pignatello, E. Oliveros, A. MacKay, Advanced oxidation processes for organic contaminant destruction based on the Fenton reaction and related chemistry, Critical Reviews in Environmental Science and Technology 36 (2006) 1–84.
[10] J. Fernandez, J. Bandara, A. Lopez, P. Albers, J. Kiwi, Efficient photo-assisted Fenton catalysis mediated by Fe ions on Nafion membranes active in the abatement of non-biodegradable azo-dye, Chemical Communications (1998) 1493–1494.
[11] J. Fernandez, M.R. Dhananjeyan, J. Kiwi, Y. Senuma, J. Hilborn, Evidence for Fenton photoassisted processes mediated by encapsulated fe ions at biocompatible pH values, Journal of Physical Chemistry B 104 (2000) 5298–5301.
[12] F.I. Hai, K. Yamamoto, K. Fukushi, Hybrid treatment systems for dye wastewater, Critical Reviews in Environmental Science and Technology 37 (2007) 315–377.
[13] C.P. Huang, Y.H. Huang, Comparison of catalytic decomposition of hydrogen peroxide and catalytic degradation of phenol by immobilized iron oxides, Applied Catalysis A: General 346 (2008) 140–148.
[14] M. Neamtu, C. Zaharia, C. Catrinescu, A. Yediler, M. Macoveanu, A. Kettrup, Fe-exchanged Y zeolite as catalyst for wet peroxide oxidation of reactive azo dye Procion Marine H-EXL, Applied Catalysis B: Environmental 48 (2004) 287–294.
[15] Z.W. Zheng, L.C. Lei, S.J. Xu, P.L. Cen, Heterogeneous UV/Fenton catalytic degradation of wastewater containing phenol with Fe–Cu–Mn–Y catalyst, Journal of Zhejiang University: Science 5 (2004) 206–211.
[16] A. Cuzzola, M. Bernini, P. Salvadori, A preliminary study on iron species as heterogeneous catalysts for the degradation of linear alkylbenzene sulphonic acids by H_2O_2, Applied Catalysis B: Environmental 36 (2002) 231–237.
[17] F. Martínez, G. Calleja, J.A. Melero, R. Molina, Iron species incorporated over different silica supports for the heterogeneous photo-Fenton oxidation of phenol, Applied Catalysis B: Environmental 70 (2007) 452–460.
[18] T. Yuranova, O. Enea, E. Mielczarski, J. Mielczarski, P. Albers, J. Kiwi, Fenton immobilized photo-assisted catalysis through a Fe/C structured fabric, Applied Catalysis B: Environmental 49 (2004) 39–50.
[19] J. Feng, X. Hu, P.L. Yue, Discoloration and mineralization of Orange II by using a bentonite clay-based Fe nanocomposite film as a heterogeneous photo-Fenton catalyst, Water Research 39 (2005) 89–96.
[20] E.G. Garrido-Ramirez, B.K.G. Theng, M.L. Mora, Clays and oxide minerals as catalysts and nanocatalysts in Fenton-like reactions – a review, Applied Clay Science 47 (2010) 182–192.
[21] M.A. De León, J. Castiglioni, J. Bussi, M. Sergio, Catalytic activity of an iron-pillared montmorillonitic clay mineral in heterogeneous photo-Fenton process, Catalysis Today 133–135 (2008) 600–605.
[22] S. Chou, C. Huang, Y.H. Huang, Heterogeneous and homogeneous catalytic oxidation by supported α-FeOOH in a fluidized-bed reactor: kinetic approach, Environmental Science and Technology 35 (2001) 1247–1251.
[23] J. Feng, X. Hu, P.L. Yue, Discoloration and mineralization of Orange II using different heterogeneous catalysts containing Fe: a comparative study, Environmental Science and Technology 38 (2004) 5773–5778.
[24] H.H. Huang, M.C. Lu, J.N. Chen, Catalytic decomposition of hydrogen peroxide and 2-chlorophenol with iron oxides, Water Research 35 (2001) 2291–2299.
[25] M.C. Lu, J.N. Chen, H.H. Huang, Role of goethite dissolution in the oxidation of 2-chlorophenol with hydrogen peroxide, Chemosphere 46 (2002) 131–136.
[26] A.L. Teel, D.D. Finn, J.T. Schmidt, L.M. Cutler, R.J. Watts, Rates of trace mineral-catalyzed decomposition of hydrogen peroxide, Journal of Environmental Engineering 133 (2007) 853–858.
[27] T.R. Gordon, A.L. Marsh, Temperature dependence of the oxidation of 2-chlorophenol by hydrogen peroxide in the presence of goethite, Catalysis Letters 132 (2009) 349–354, doi:10.1007/s10562-009-0125-6.
[28] M.D. Gurol, S.S. Lin, Hydrogen peroxide/iron oxide-induced catalytic oxidation of organic compounds, Water Science and Technology: Water Supply 1 (2001) 131–138.
[29] S.S. Lin, M.D. Gurol, Catalytic decomposition of hydrogen peroxide on iron oxide: kinetics, mechanism, and implications, Environmental Science and Technology 32 (1998) 1417–1423.

[30] Y.T. Lin, M.C. Lu, Catalytic action of goethite in the oxidation of 2-chlorophenols with hydrogen peroxide, Water Science and Technology 55 (12) (2007) 101–106.
[31] Z. Han, Y. Dong, S. Dong, Copper-iron bimetal modified PAN fiber complexes as novel heterogeneous Fenton catalysts for degradation of organic dye under visible light irradiation, Journal of Hazardous Materials 189 (2011) 241–248.
[32] M.I. Litter, Introduction to photochemical advanced oxidation processes for water treatment, in: The Handbook of Environmental Chemistry, Springer-Verlag, Berlin/Heidelberg, 2005, pp. 325–366.
[33] M.E. Morgada, I.K. Levy, V. Salomone, S.S. Farías, G. López, M.I. Litter, Arsenic (V) removal with nanoparticulate zerovalent iron: effect of UV light and humic acids, Catalysis Today 143 (2009) 261–268.
[34] P. Raja, A. Bozzi, W.F. Jardim, G. Mascolo, R. Renganathan, J. Kiwi, Reductive/oxidative treatment with superior performance relative to oxidative treatment during the degradation of 4-chlorophenol, Applied Catalysis B: Environmental 59 (2005) 249–257.
[35] D.H. Bremner, A.E. Burgess, D. Houllemare, K.C. Namkung, Phenol degradation using hydroxyl radicals generated from zero-valent iron and hydrogen peroxide, Applied Catalysis B: Environmental 63 (2006) 15–19.
[36] R. Cheng, J.l. Wang, W.x. Zhang, Comparison of reductive dechlorination of p-chlorophenol using Fe^0 and nanosized Fe^0, Journal of Hazardous Materials 144 (2007) 334–339.
[37] L.G. Devi, S. Girish Kumar, K. Mohan Reddy, C. Munikrishnappa, Photo degradation of methyl orange an azo dye by advanced Fenton process using zero valent metallic iron: influence of various reaction parameters and its degradation mechanism, Journal of Hazardous Materials 164 (2009) 459–467.
[38] T. Zhou, Y. Li, J. Ji, F.S. Wong, X. Lu, Oxidation of 4-chlorophenol in a heterogeneous zero valent iron/H_2O_2 Fenton-like system: kinetic, pathway and effect factors, Separation and Purification Technology 62 (2008) 551–558.
[39] M. Barreto-Rodrigues, F.T. Silva, T.C.B. Paiva, Combined zero-valent iron and Fenton processes for the treatment of Brazilian TNT industry wastewater, Journal of Hazardous Materials 165 (2009) 1224–1228.
[40] L. Xu, J. Wang, A heterogeneous Fenton-like system with nanoparticulate zero-valent iron for removal of 4-chloro-3-methyl phenol, Journal of Hazardous Materials 186 (2011) 256–264.
[41] C.H. Liao, S.F. Kang, Y.W. Hsu, Zero-valent iron reduction of nitrate in the presence of ultraviolet light, organic matter and hydrogen peroxide, Water Research 37 (2003) 4109–4118.
[42] Y. Nie, C. Hu, L. Zhou, J. Qu, Q. Wei, D. Wang, Degradation characteristics of humic acid over iron oxides/Fe^0 core-shell nanoparticles with UVA/H_2O_2, Journal of Hazardous Materials (2010).
[43] H.S. Son, J.K. Im, K.D. Zoh, A Fenton-like degradation mechanism for 1,4-dioxane using zero-valent iron (Fe^0) and UV light, Water Research 43 (2009) 1457–1463.
[44] C.S. Zalazar, M.D. Labas, C.A. Martin, R.J. Brandi, A.E. Cassano, Reactor scale-up in AOPs: from laboratory to commercial scale, Water Science and Technology (2004) 13–18.
[45] US Department of Health and Human, Toxicilogical Profile for Chlorophenols, U.S. Department of Health and Human Services; Public Health Service Agency for Toxic Substances and Disease Registry, U.S Government Printing Office, Washington, DC, 1999.
[46] American Public Health Association, Standard Methods for the Examination of Water and Wastewater, 19th ed., Washington DC, USA, 1995.
[47] A.O. Allen, C.J. Hochanadel, J.A. Ghormley, T.W. Davis, Decomposition of water and aqueous solutions under mixed fast neutron and gamma radiation, Journal of Physical Chemistry 56 (1952) 575–586.
[48] Y.-P. Sun, X.-q. Li, J. Cao, W.-x. Zhang, H.P. Wang, Characterization of zero-valent iron nanoparticles, Advances in Colloid and Interface Science 120 (2006) 47–56.
[49] Z. Fang, J. Chen, X. Qiu, X. Qiu, W. Cheng, L. Zhu, Effective removal of antibiotic metronidazole from water by nanoscale zero-valent iron particles, Desalination 268 (2011) 60–67.
[50] D. Rosicka, J. Sembera, Assessment of influence of magnetic forces on aggregation of zero-valent iron nanoparticles, Nanoscale Research Letters 6 (2011) 6–10.
[51] J.A. Bergendahl, T.P. Thies, Fenton's oxidation of MTBE with zero-valent iron, Water Research 38 (2004) 327–334.
[52] R. Chen, J.J. Pignatello, Role of quinone intermediates as electron shuttles in Fenton and photoassisted Fenton oxidations of aromatic compounds, Environmental Science and Technology 31 (1997) 2399–2406.
[53] R. Chen, J.J. Pignatello, Structure–activity study of electron-shuttle catalysis by quinones in the oxidation of aromatic compounds by the Fenton reaction, Journal of Advanced Oxidation Technologies 4 (1999) 447–453.
[54] A.E. Cassano, C.A. Martin, R.J. Brandi, O.M. Alfano, Photoreactor analysis and design: fundamentals and applications, Industrial and Engineering Chemistry Research 34 (1995) 2155–2201.
[55] M.N. Ozisik, Radiative Transfer and Interactions with Conduction and Convection, J. Wiley, New York, 1973.
[56] G.B. Ortiz de la Plata, O.M. Alfano, A.E. Cassano, Optical properties of goethite catalyst for heterogeneous photo-Fenton reactions: comparison with a titanium dioxide catalyst, Chemical Engineering Journal 137 (2008) 396–410.
[57] J.J. Duderstadt, R. Martin, Transport Theory, Wiley, New York, 1979.
[58] K.A. Levenberg, Method for the solution of certain problems in least squares, Quarterly of Applied Mathematics 2 (1944) 164–168.
[59] D. Marquardt, An algorithm for least-squares estimation of nonlinear parameters, SIAM Journal on Applied Mathematics 11 (1963) 431–441.
[60] M.L. Satuf, R.J. Brandi, A.E. Cassano, O.M. Alfano, Experimental method to evaluate the optical properties of aqueous titanium dioxide suspensions, Industrial and Engineering Chemistry Research 44 (17) (2005) 6643–6649.
[61] H.C. van de Hulst, Multiple Light Scattering, Academic Press, 1980.
[62] M.I. Cabrera, O.M. Alfano, A.E. Cassano, Absorption and scattering coefficients of titanium dioxide participate suspensions in water, Journal of Physical Chemistry 100 (1996) 20043–20050.
[63] M.d.l.M. Ballari, R. Brandi, O. Alfano, A. Cassano, Mass transfer limitations in photocatalytic reactors employing titanium dioxide suspensions. I. Concentration profiles in the bulk, Chemical Engineering Journal 136 (2008) 50–65.
[64] G. Camera Roda, F. Santarelli, A rational approach to the design of photocatalytic reactors, Industrial & Engineering Chemistry Research 46 (2007) 7637–7644.